Desalination and Water Treatment
www.deswater.com

doi: 10.5004/dwt.2021.26451

209 (2021) 230–241
January

A novel Al^0-CNTs-Fe_3O_4 for the removal of low concentration sulfamethoxazole from aqueous solution by a couple of adsorption and degradation processes

Yunbo Liu[a], Jing Tian[a], Ruofan Pu[a], Bingqing Wang[a], Baohua An[a], Yong Liu[a,b,*]

[a]*College of Chemistry and Materials Science, Sichuan Normal University, Chengdu 610066, China, emails: liuyong75@sicnu.edu.cn (Y. Liu), 302716045@qq.com (Y. Liu), wltian@sicnu.edu.cn (J. Tian), 823530473@qq.com (R. Pu), 525675064@qq.com (B. Wang), 2060252023@qq.com (B. An)*
[b]*Key Laboratory of Treatment for Special Wastewater of Sichuan Province Higher Education System, Sichuan, Chengdu 610066, China*

Received 20 March 2020; Accepted 11 August 2020

ABSTRACT

A novel composite (Al^0-CNTs-Fe_3O_4), synthesized through sintering and co-precipitation, was used to remove low concentration sulfamethoxazole (SMZ) in wastewater with a two-step process (adsorption followed by oxidation). Briefly, SMZ was firstly adsorbed on the surface of Al^0-CNTs-Fe_3O_4 at initial pH of 3 (the adsorption process), then the adsorbed SMZ was degraded by the Al^0-CNTs-Fe_3O_4/O_2 system with 3 g/L Al^0-CNTs-Fe_3O_4 and initial pH of 1.5 (the degradation process). With the two-step process, 99.6% of the SMZ was degraded within 10 min while only 68.5% degraded with the one-step process (simultaneous adsorption and degradation). The Langmuir model and pseudo-second-order kinetic model could describe well the adsorption behavior of SMZ on Al^0-CNTs-Fe_3O_4. The maximum adsorption capacity (Q_{max}) calculated from the Langmuir isotherm model and the adsorption rate constant (K_2) calculated from the pseudo-second-order kinetic model were 17.497 mg/g and 0.192 g/(mg min) (T = 298 K, pH = 3.0), respectively. Moreover, the saturated Al^0-CNTs-Fe_3O_4 was easily separated from the aqueous solution due to its saturation magnetization (Ms) value of 35.14 emu/g, which was convenient for the subsequent degradation process. Possible mechanisms of the adsorption and degradation of SMZ by Al^0-CNTs-Fe_3O_4 were also proposed.

Keywords: Adsorption; Contaminants degradation; Fenton-like; Antibiotics; Advanced oxidation processes

1. Introduction

Sulfonamides are the drugs with the structure of *p*-aminobenzenesulfonamide [1], which have been widely used to prevent animal diseases [2,3]. As one of the most common sulfonamides, sulfamethoxazole (SMZ) is broadly used to kill various bacteria (e.g., Listeria mono-cytogenes and *Escherichia coli*), and to remedy bacterial infections such as prostatitis, urinary tract infections, and bronchitis [4,5]. Recently, SMZ has been detected in rivers, lakes, and effluents of urban sewage treatment plants. Since SMZ in the environment is often accompanied by a certain ecological toxicity and potential harm to environmental biosafety [6–8], the removal of SMZ from aqueous solution has received many concerns. In order to reduce the harm of antibiotic pollution in the environment to ecosystem and human health, many methods have been developed to remove antibiotics, such as advanced oxidation processes (AOPs), adsorption, membrane technology, biological degradation processes, etc. [9].

Sulfonamides can be degraded by AOPs with *in-situ* generated $^\bullet$OH radicals as the main oxidation species [10,11]. Fenton oxidation process, as one of the AOPs, is believed to be efficient for the removal of sulfonamides in aqueous solution due to its mild reaction condition and simple operating process [12,13]. However, the difficulty in recycling

---

* Corresponding author.

Fe^{2+} hinders the application of the traditional Fenton process. To overcome this weakness, a Fenton-like process using Fe_3O_4 as the catalyst was developed and attracted many attentions due to its low cost, high catalytic efficiency, and catalyst recyclability [14–16]. In the traditional Fenton process, the H_2O_2 in aqueous solution is always provided by bulk commercial H_2O_2, which brings safety risk to the transportation and storage of H_2O_2, and also reduces the H_2O_2 utilization efficiency in the degradation of organic contaminants [17,18]. Recently, a high efficient process of *in-situ* generation of H_2O_2 by metal-carbon nanotubes (CNTs) composites, such as Zn^0-CNTs, Mg^0-CNTs, and Al^0-CNTs, reacting with O_2 has been achieved [19,20]. Therefore, considering the advantages of Fenton-like catalyst and *in-situ* generation of H_2O_2 in Fenton process, a novel Fenton-like process in which $^\bullet OH$ radicals were generated from the activation of O_2 in solution by catalyst had been developed [21–23].

Most sulfonamides in wastewater are in trace or low concentrations with low mass transfer rates, which results in the low degradation efficiency of sulfonamides by Fenton-like oxidation process. To this end, Fenton-like catalysts with adsorption properties have been developed to improve the degradation efficiency of organic contaminants. It is well-known that CNTs are good adsorbents for pollutant removal due to their high specific surface areas as nanomaterials and the hollow nanostructures [24]. In addition, CNTs can be used as the supports of catalysts due to their perfect thermal, chemical, electrical, or mechanical performances [25]. Therefore, CNTs based Fenton-like catalysts are proposed to have both adsorption and catalysis performances.

In the traditional Fenton-like process, the adsorption and degradation of organic contaminants are carried out simultaneously in a single system (one-step process). However, this one-step process cannot ensure that the adsorption and degradation are conducted at their most appropriate conditions. If the adsorption and degradation of organic contaminants are proceeded at two stepwise systems: degradation after adsorption (two-step process) in the Fenton-like process, the degradation efficiency of organic contaminants is likely to be significantly improved by making the two systems in their optimal conditions.

In this work, a novel Al^0-CNTs-Fe_3O_4 composite capable of activating O_2 to *in-situ* generated H_2O_2/$^\bullet OH$ was synthesized and used for the removal of SMZ through a two-step process. The main purposes of this paper are: (1) to study the adsorption behaviors of SMZ on Al^0-CNTs-Fe_3O_4 (adsorption isotherms, adsorption kinetics, the effect of initial pH, possible adsorption mechanisms, etc.); (2) to investigate the degradation efficiency of SMZ by Al^0-CNTs-Fe_3O_4/O_2 system (the effect of Al^0-CNTs-Fe_3O_4 dosage and possible degradation pathways); and (3) to compare the one-step process with two-step process for the degradation of SMZ.

2. Materials and methods

2.1. Materials

CNTs (5–15 nm) were purchased from Timesnano (Chengdu, China). SMZ (99.0%) from Damas-Beta Company was purchased from China. Aluminum powder (2.70 g/cm^3, 38–75 μm, and 99.0%) and polyethylene glycol (PEG) 4000 (99.0%) were obtained from the National Medicines Corporation Ltd., China. Deionized water was applied to all experiments.

2.2. Synthesis of Al^0-CNTs-Fe_3O_4

The Al^0-CNTs-Fe_3O_4 was synthesized by a high-temperature sintering combined with co-precipitation process. In detail, aluminum powder and CNTs with mass ratio of 10:1 were added into a ball mill tank and ball-milled for 2 h; the obtained mixture was then sintered in a ThermConcept for 1 h at 973 K. After cooling down the sinters, the Al^0-CNTs composite was obtained. Then, the as-prepared Al^0-CNTs was added quickly into a solution containing Fe^{3+} and Fe^{2+} ions at a molar ratio of 1:1.5; the initial pH of the suspension solution was adjusted to 9 with 2 mol/L ammonia. After a 15 min reaction, the solids in the suspension solution were separated, washed by deionized water to neutrality, and placed in a freeze dryer for 24 h to obtain Al^0-CNTs-Fe_3O_4. All the above reactions were carried out under argon protection.

2.3. Material characterizations and chemical analyses

The morphology of Al^0-CNTs-Fe_3O_4 was characterized by a scanning electron microscopy (SEM Hitachi JEM-7500F, Japan). Crystalline structures of Al^0-CNTs-Fe_3O_4 was performed on an X-ray diffractometer (Bruker D8 Adv., Germany). The functional groups of Al^0-CNTs-Fe_3O_4 were recorded by Fourier transform infrared (FT-IR) spectrometer (VERTEX 70) with a spectra range of 400–4,000 cm^{-1}.

The H_2O_2 concentrations were determined by a UV-vis spectrophotography (Alpha-1500, China) using $K_2TiO(C_2O_4)_2$ as the color indicator at a wavelength of 400 nm. The SMZ concentrations were determined by ultra performance liquid chromatography (UPLC) (Agilent 1290, California, USA), in which the mobile phase was acetonitrile and 0.1% formic acid solution (35/65, v/v) at a flow rate of 0.2 mL/min; analytical wavelength and the column temperature were set as 270 nm and 308 K, respectively.

2.4. Determination of the point of zero charge of Al^0-CNTs-Fe_3O_4

The determination of the point of zero charge of Al^0-CNTs-Fe_3O_4 was conducted using a usual method in the literature [26]. First, the pH of 25 mL suspensions containing Al^0-CNTs-Fe_3O_4 and deionized water were adjusted to 1–10 with 0.1 mol/L HCl and NaOH. The initial pH of the suspensions were measured after 20 min agitation for equilibrium. Then, the suspensions were added 1.5 g $NaNO_3$ and agitated for another 4 h to determine the final pH. The experiment data were plotted as ΔpH (final pH − initial pH) against initial pH.

2.5. Batch adsorption experiments

To investigate the adsorption behavior of SMZ on Al^0-CNTs-Fe_3O_4, the effects of initial pH (1–11), reaction temperature (298–318 K), and contact time (0–120 min) on the adsorption of SMZ were evaluated by the batch adsorption experiments. All of adsorption experiments were carried out under N_2 protection. After adding required amount of Al^0-CNTs-Fe_3O_4 into a 250 mL glass bottle containing SMZ solution, the glass bottle was placed in a constant temperature oscillator box, and oscillated at a rotation rate of 170 rpm. The solution was taken out at a given time interval and filtered with a 0.22 μm membrane. The concentration of SMZ in the filtrates was determined by UPLC.

2.6. Adsorption kinetics

The adsorption kinetic experiments were carried out at the temperature of 298 K, the SMZ concentrations at 5–25 mg/L, the Al^0-CNTs-Fe_3O_4 dosage at 0.8 g/L, and the initial pH of 3.

The amount of SMZ adsorbed at time *t* noted as q_t (mg/g) is defined as Eq. (1):

$$q_t = \frac{\left(c_0 - c_t\right) \times V}{M} \tag{1}$$

where c_0 (mg/L) and c_t (mg/L) are the initial and remaining concentrations of SMZ, respectively. *V* (L) is the solution volume, and *M* (g) is the mass of Al^0-CNTs-Fe_3O_4.

The obtained kinetic equilibrium data were simulated by the pseudo-first-order kinetic model, pseudo-second-order kinetic model, intra-particle diffusion, and Elovich models (Eqs. (2)–(5)), respectively [27].

$$\log\left(q_e - q_t\right) = \log q_e - \frac{k_1}{2.303} t \tag{2}$$

$$\frac{1}{q_t} = \frac{1}{k_2 q_e^2} \cdot \frac{1}{t} + \frac{t}{q_e} \tag{3}$$

$$q_t = k_d t^{1/2} + d \tag{4}$$

$$q_t = \frac{1}{\beta_E} \cdot \ln\left(\alpha_E \beta_E\right) + \frac{1}{\beta_E} \ln t \tag{5}$$

where q_e (mg/g) is the amount of SMZ adsorbed at equilibrium time, k_1 (1/min), k_2 (g/(mg min)), and k_d (mg/(g min$^{1/2}$)) are the rate constants in the pseudo-first-order kinetic model, pseudo-second-order kinetic model, and intra-particle diffusion model, respectively. *d* is a dimensionless constant correlated to the thickness of boundary layer. α_E (mg/g min) and β_E (g/mg) are the initial adsorption rate constant and the desorption constant, respectively.

2.7. Adsorption isotherms

Adsorption isotherm experiments were carried out at the initial pH of 3, the SMZ initial concentration of 2.5 mol/L, the Al^0-CNTs-Fe_3O_4 dosage of 0.8 g/L, and the temperature of 298–318 K. The data obtained from the adsorption isotherm experiments were analyzed by Langmuir isotherm model, Freundlich isotherm model, Temkin, and Dubinin–Radushkevich model [Eqs. (6)–(11)] [27].

$$\frac{c_e}{q_e} = \frac{1}{Q_{\max} b} + \frac{c_e}{Q_{\max}} \tag{6}$$

$$\log q_e = \log K_F + \frac{1}{n} \log c_e \tag{7}$$

$$q_e = B_1 \ln K_T + B_1 \ln c_e \tag{8}$$

$$\ln q_e = \ln Q_{\max} - \beta \varepsilon^2 \tag{9}$$

$$\varepsilon = RT \ln\left(1 + \left(\frac{1}{c_e}\right)\right) \tag{10}$$

$$E = \frac{1}{\left(2\beta\right)^{1/2}} \tag{11}$$

where c_e (mg/L) is the concentration of SMZ at equilibrium, $Q_{\max}$ (mg/g) is the maximum adsorption capacity. *b* (L/mg) and β (mol^2/kJ^2) are the Langmuir constant and the Dubinin–Radushkevich constant, respectively, associated with the adsorption energy. K_F and *n* are two Freundlich constants about the adsorption capacity of adsorbent and the degree of adsorption feasibility. K_t (L/mg) and B_1 are the Temkin constant and the constant about the heat of adsorption, respectively. ε and *E* (kJ/mol) are the adsorption potential and the free energy of adsorption, respectively.

To understand the thermodynamic behavior of SMZ adsorption onto Al^0-CNTs-Fe_3O_4, the thermodynamic parameters were calculated by the following equations [28,29]:

$$\Delta G^\circ = -RT \ln K^\circ \tag{12}$$

$$K^\circ = 55.5 \left(\frac{1{,}000}{c} b\right) \tag{13}$$

$$\ln K^\circ = -\frac{\Delta H^\circ}{RT} + \frac{\Delta S^\circ}{R} \tag{14}$$

where ΔG° (kJ/mol), ΔH° (kJ/mol), and ΔS° (kJ/(mol K)) are the Gibbs free energy change, the enthalpy change, and the entropy change, respectively. *T* (K) is the absolute temperature; *R* (8.314 J/mol K) is the gas constant; K^0 is a dimensionless constant from *b* (the Langmuir constant); 55.5 (mol/L) is the mole of water per liter of aqueous solution, and *c* is the molecular weight of SMZ.

2.8. Degradation of SMZ

2.8.1. Degradation of SMZ by Al^0-CNTs-Fe_3O_4/O_2 system

Firstly, SMZ in the 100 mL solution with an initial concentration 2.5 mg/L was adsorbed onto 0.8 g/L Al^0-CNTs-Fe_3O_4 at 298 K and initial pH of 3. Secondly, the SMZ-saturated Al^0-CNTs-Fe_3O_4 was separated from the solution with a magnet and dried for 12 h. Then, the SMZ-saturated Al^0-CNTs-Fe_3O_4 was added into the H_2SO_4 solution at initial pH of 1.5 with solid to water ratio of 3.0 g/L. Afterwards, O_2 was purged into the H_2SO_4 solution at 200 mL/min. The SMZ adsorbed on the Al^0-CNTs-Fe_3O_4 would be degraded by the oxidizing species from the reaction of Al^0-CNTs-Fe_3O_4 with O_2.

During the removal of SMZ by the adsorption–degradation process, the mass of SMZ adsorbed on the Al^0-CNTs-Fe_3O_4 was obtained from the mass difference of SMZ in solution before and after adsorption. The degradation efficiency of SMZ on the Al^0-CNTs-Fe_3O_4 was calculated by the mass difference of SMZ on the Al^0-CNTs-Fe_3O_4 before and after degradation. The mass of SMZ on the Al^0-CNTs-Fe_3O_4 after degradation was obtained as follows: the Al^0-CNTs-Fe_3O_4 after degradation was washed thoroughly by 0.05 mol/L HCl and then SMZ in the eluent was detected.

2.8.2. Control experiments of SMZ degradation

To further understand the pathways and mechanisms of the degradation of SMZ in the Al^0-CNTs-Fe_3O_4/O_2 system, control experiments were carried out in Al^0-CNTs/O_2, Al^0-CNTs-Fe_3O_4/O_2, and Al^0-CNTs-Fe_3O_4/TBA (*tert*-butyl alcohol)/O_2 systems, respectively, at initial pH of 1.5 with 2.55 g/L Al^0-CNTs or 3 g/L Al^0-CNTs-Fe_3O_4. 0.1 mol/L HCl and NaOH were used to adjust the initial pH. To investigate the function of $^{\bullet}OH$ radical, TBA was introduced into the Al^0-CNTs-Fe_3O_4/O_2 system as the quencher of $^{\bullet}OH$ [30,31]. Moreover, the accumulated concentrations of H_2O_2 in the Al^0-CNTs/O_2 system and the Al^0-CNTs-Fe_3O_4/O_2 system were also measured by UV-vis.

2.9. Comparison of one-step and two-step processes for the degradation of SMZ

In the one-step process, 0.8 g/L Al^0-CNTs-Fe_3O_4 was added to 100 mL solution with an SMZ initial concentration of 2.5 mg/L at initial pH of 1.5, the adsorption and degradation of SMZ would simultaneously occur in the atmosphere of O_2. During the two-step process, the same amount of Al^0-CNTs-Fe_3O_4 used in the one-step process was added to the solution containing the same concentration of SMZ at initial pH of 3. After the adsorption process, the SMZ was then degraded in the Al^0-CNTs-Fe_3O_4/O_2 system with the O_2 flow rate at 200 mL/min, solid to water ratio at 3.0 g/L and initial pH at 1.5.

3. Results and discussion

3.1. Characterization of Al^0-CNTs-Fe_3O_4

3.1.1. Scanning electron microscopy, energy-dispersive spectroscopy, and vibrating sample magnetometer

The morphology of Al^0-CNTs-Fe_3O_4 was obtained from SEM images. It can be clearly seen from Fig. 1a that the Al^0-CNTs-Fe_3O_4 had a porous and loose network structure, which favored its adsorption of SMZ. The image in Fig. 1b shows the highly entangled nature of CNTs. Additionally, it can be seen from the energy dispersive spectra (EDS) of Al^0-CNTs-Fe_3O_4 (Fig. 1c) that the relative contents of Al, C, Fe, and O were 55.84%, 9.00%, 13.35%, and 21.81%, respectively. Moreover, almost no hysteresis loop could be observed in the room temperature magnetization curve in Fig. 1d. The saturation magnetization (Ms) values of Al^0-CNTs-Fe_3O_4 was 35.14 emu/g. The good magnetic property allowed Al^0-CNTs-Fe_3O_4 to be easily separated from water.

3.1.2. Brunauer–Emmett–Teller

The Brunauer–Emmett–Teller (BET) surface area and pore size distribution of Al^0-CNTs-Fe_3O_4 and CNTs were evaluated by the N_2 adsorption–desorption isotherms and the BJH (Barrett–Joyner–Halenda) analysis (Fig. 2). The average pore size and the BET specific surface area of Al^0-CNTs-Fe_3O_4 were determined to be 33.08 nm and 58.97 m^2/g, respectively, while that of the CNTs were 30.21 nm and 104.97 m^2/g, respectively. The N_2 adsorption–desorption curves showed that the Al^0-CNTs-Fe_3O_4 and CNTs could be described by type IV isotherm with a H3 hysteresis loop, which indicated that Al^0-CNTs-Fe_3O_4 and CNTs were intricated mesoporous and microporous materials with pores of plate structure [32]. It also indicated that the structure of CNTs did not change obviously after being loaded by Al^0 and Fe_3O_4.

3.1.3. FTIR and XRD

The FT-IR spectrums of Al^0-CNTs-Fe_3O_4 before and after adsorption were shown in Fig. 3. As can be seen from Fig. 3a, the peaks at 1,620 and 1,150 cm^{-1} were attributed to stretching vibrations of C=O and C–O group [33], respectively. The corresponding peaks at 3,400 and 1,380 cm^{-1} were associated with the –OH on the CNTs [34]. In addition, the peaks of C–O and –OH were weakened after the adsorption of SMZ by Al^0-CNTs-Fe_3O_4 (Fig. 3b), which might be caused by the electron–donor–acceptor (EDA) interaction between Lewis basic sites of SMZ (–NH and $-NH_2$) and free electrons of CNTs [35].

The XRD patterns of Al^0-CNTs-Fe_3O_4 before and after degradation of SMZ are shown in Figs. 3c and d. The diffraction peaks at 38.47°, 44.74°, 65.13°, 78.23°, and 82.44° were the peaks of Al^0 (PDF #04–0787). The peaks at 60.25°, 35.6°, 43.14°, 53.54°, 57.34°, and 62.82° were corresponded to Fe_3O_4 (PDF #65–3107) and 62.73° was assigned to the structure of C (PDF #46–0944). The weak diffraction peaks of Fe_3O_4 might be due to the cover of Fe_3O_4 by Al^0 or the low content of Fe_3O_4 in Al^0-CNTs-Fe_3O_4 sample [36]. These results proved that Fe_3O_4 and Al^0 were successfully loaded on CNTs. Compared to the peaks of Al^0-CNTs-Fe_3O_4 before degradation, the peaks belonging to Al^0 disappeared in Al^0-CNTs-Fe_3O_4 after degradation, which indicated that Al^0 was consumed during degradation. In addition, the peaks attributed to Fe_3O_4 were substantially existing in the sample after degradation, which implied that little loss of Fe_3O_4 occurred in the degradation of SMZ.

3.2. Adsorption of SMZ on Al^0-CNTs-Fe_3O_4

3.2.1. Effects of initial pH on SMZ adsorption

The influence of initial pH on SMZ removal by Al^0-CNTs-Fe_3O_4 is shown in Fig. 4a. The removal efficiency of SMZ increased markedly with the increased pH from 1 to 3, and the highest efficiency was obtained at pH of 3 (91.18%). Then, the SMZ removal decreased rapidly when pH continually increased from 3 to 5, followed by a slight decrease at pH from 5 to 11. It was confirmed that the hydrophilicity, ionization and solubility were always seriously responsible for the adsorption behaviors [37–40]. There are two pk_a values (pk_{a1} = 1.97 and pk_{a2} = 6.16 [41]) of SMZ due to the presence of $-NH_2$ and –COOH. Therefore, there would be three forms of SMZ [42]: positively charged

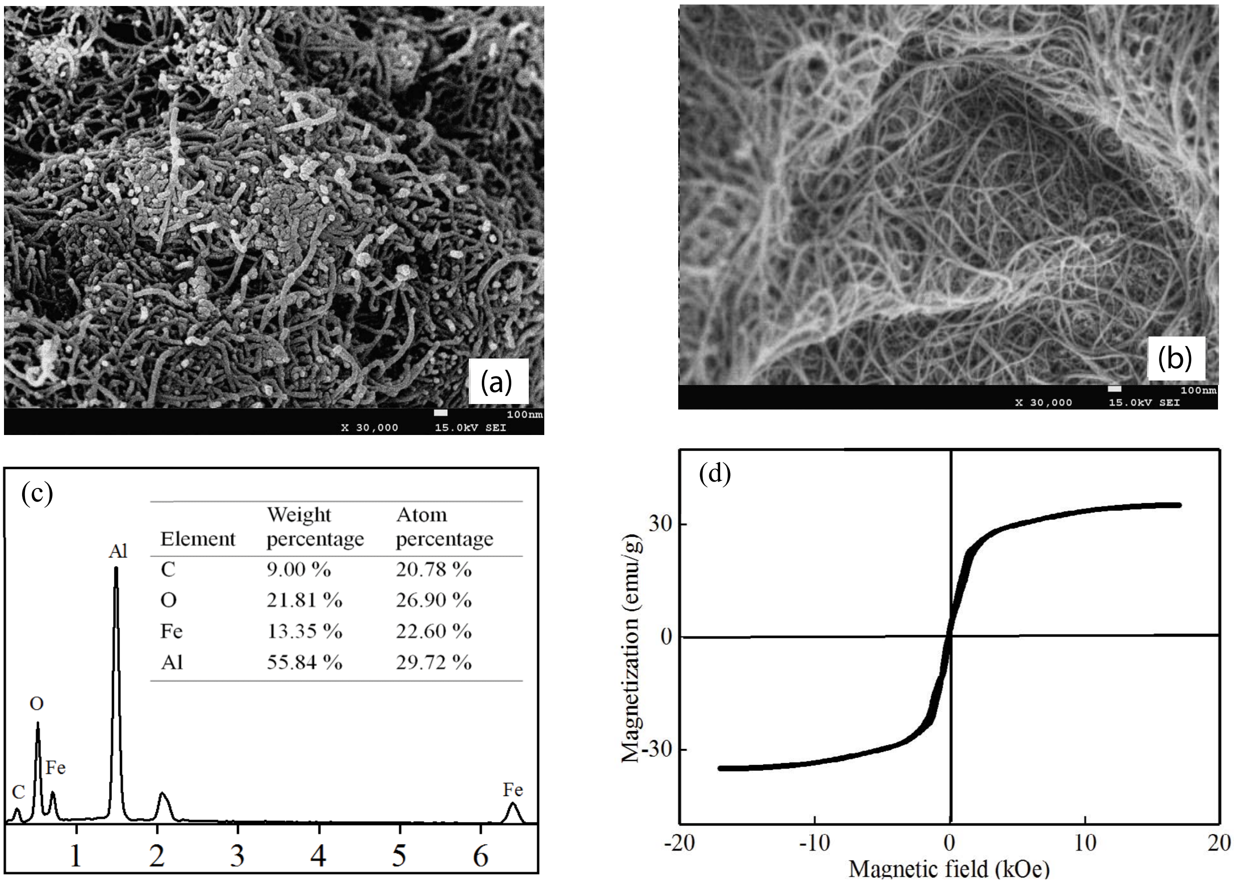

Fig. 1. SEM images of Al^0-CNTs-Fe_3O_4 (a) and CNTs (b); EDX spectra (c) and magnetic hysteresis loops (d) of Al^0-CNTs-Fe_3O_4.

form when pH was less than 1.97, both positively and negatively charged form when pH was between 1.97 and 6.19, and negative charged form when pH was greater than 6.19. The point of zero charge of Al^0-CNTs-Fe_3O_4 was determined to be 3.9 (the initial pH at which the ΔpH equaled to 0 (Fig. 4b) [32]). This result implied that the Al^0-CNTs-Fe_3O_4 was positively charged at pH < 3.9 and negatively charged at pH > 3.9. When the pH of the solution was less than 2 or greater than 6, a strong electrostatic repulsion force would form between SMZ and Al^0-CNTs-Fe_3O_4 due to the same positively or negatively electric charges, which resulted in low adsorption efficiencies at pH < 2 or >6 [43]. Therefore, the highest adsorption efficiency was achieved at an initial pH of 3 due to the electrostatic interaction between the positively charged Al^0-CNTs-Fe_3O_4 and negatively charged SMZ. Moreover, at relatively low pH, the hydrogen-bonding forces between the $-NH_2$ or –COOH groups of SMZ and the –OH on the CNTs were enhanced [44], which also favored the adsorption of SMZ on Al^0-CNTs-Fe_3O_4.

3.2.2. Isotherm models

The Langmuir isotherm model describes that a single-layer adsorption reaction occurs at a certain number of active sites, and there are no intermolecular interactions between adsorbed molecules or adjacent sites [45]. The Freundlich isotherm model was used to describe the adsorption characteristics for heterogeneous surfaces and multilayer adsorption, and the adsorption affinity and heat are unevenly distributed over the surface [46]. Temkin model describes the interaction of adsorbate-adsorbate and the Dubinin–Radushkevich model characterizes whether the adsorption process is chemical adsorption or physical adsorption.

The calculated parameters by the Langmuir isotherm model, Freundlich isotherm model, Temkin model, and Dubinin–Radushkevich model are shown in Table 1 and the plot of c_e vs. q_e is shown in Fig. 5. It can be seen from Fig. 5 that the adsorption capacity decreased with the increase of temperature. The maximum adsorption capacities at 298, 308, and 318 K were 17.50, 17.32, and 14.92 mg/g, respectively. The results in Table 1 also show that the Langmuir model could describe well the adsorption of SMZ on Al^0-CNTs-Fe_3O_4 according to the high R^2 (>0.99), which indicated that the adsorption of SMZ on Al^0-CNTs-Fe_3O_4 was dominated by monolayer adsorption and the active sites were uniformly distributed on the surface of the Al^0-CNTs-Fe_3O_4.

3.2.3. Thermodynamics

The thermodynamic data calculated by Eqs. (12)–(14) were used to further evaluate the adsorption behavior. The calculated thermodynamic data for the adsorption of SMZ on Al^0-CNTs-Fe_3O_4 are shown in Table 2. The obtained

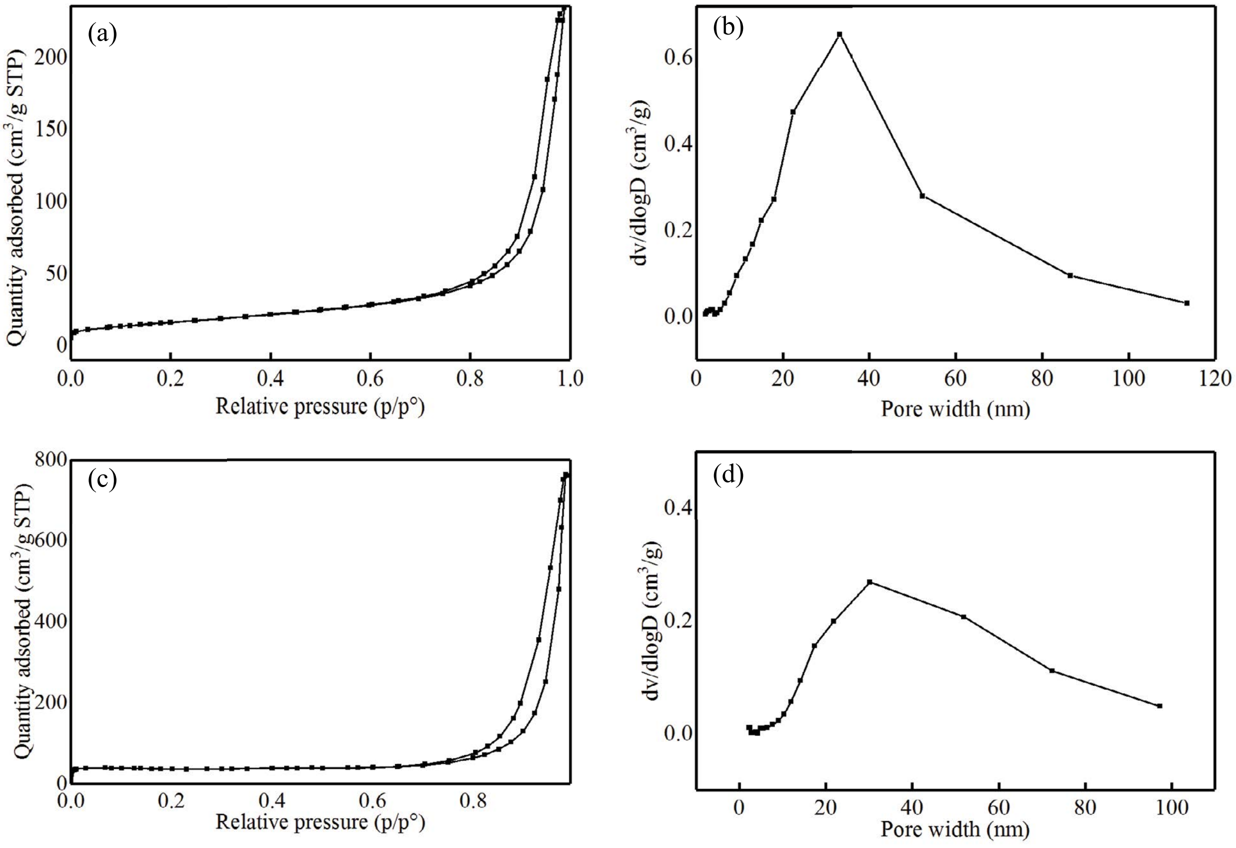

Fig. 2. N_2 adsorption–desorption isotherms and pore size distributions of Al^0-CNTs-Fe_3O_4 (a and b) and CNTs (c and d).

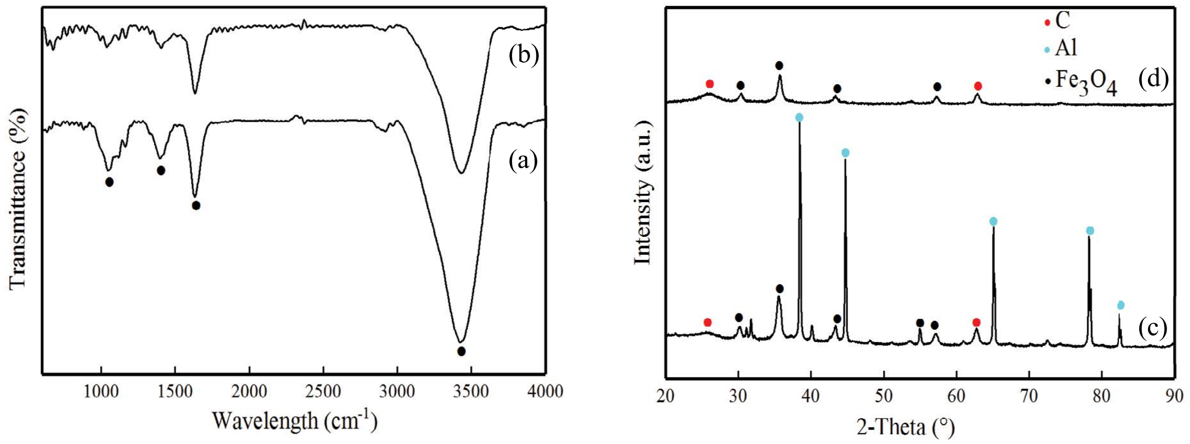

Fig. 3. FTIR spectra of fresh Al^0-CNTs-Fe_3O_4 (a) and Al^0-CNTs-Fe_3O_4 after adsorption (b); XRD patterns of Al^0-CNTs-Fe_3O_4 before (c) and after (d) the degradation of SMZ.

negative $\Delta G°$ values indicated that the adsorption process was feasible and spontaneous. The obtained positive value of $\Delta S°$ suggested that the system randomness increased during the adsorption process of SMZ onto Al^0-CNTs-Fe_3O_4. Moreover, the negative value of $\Delta H°$ suggested the adsorption process was exothermic [28,47], which also confirmed by the increase of the adsorption efficiency of SMZ with the decrease of temperature.

3.2.4. Adsorption kinetics

To better understand the adsorption mechanism, experimental data were simulated by pseudo-first-order kinetic, pseudo-second-order kinetic, intra-particle diffusion, and Elovich models, respectively. Pseudo-first-order kinetic model, pseudo-second-order kinetic model, and Elovich model are used to investigate the reaction pathway and

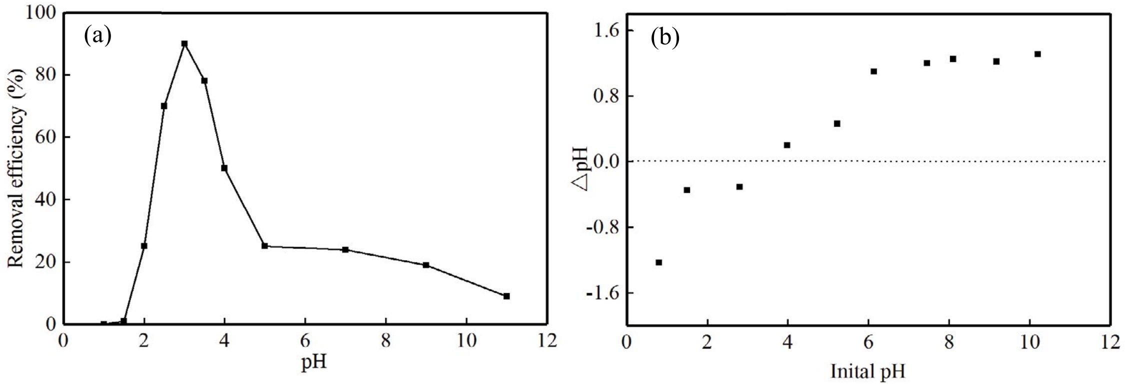

Fig. 4. Effects of initial pH on removal of SMZ (a) (initial SMZ concentration = 2.5 mg/L, adsorbent dosage = 0.8 g/L, reaction temperature = 298 K, and reaction time = 90 min) and the point of zero charge analysis of Al^0-CNTs-Fe_3O_4 (b).

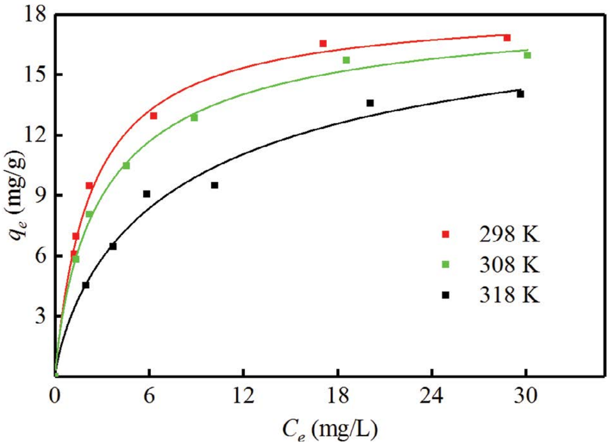

Fig. 5. Adsorption isotherms of SMZ on Al^0-CNTs-Fe_3O_4 (Al^0-CNTs-Fe_3O_4 = 0.8 g/L, contact time = 60 min, and initial pH = 3).

the adsorption rate-limiting step. The parameters of the intra-particle diffusion model are related to the adsorption boundary layer thickness. The fitting results of kinetics parameters by four models are summarized in Table 3. It was obvious that the adsorption removal of SMZ was found to be quite rapid at the initial 5 min and reach equilibrium at about 20 min (Fig. 6). Fig. 6 also shows that the higher concentration of SMZ had a higher adsorption capacity, which might be due to that high concentration of SMZ had a stronger driving force for the migration of SMZ from solution to the surface boundary layers of the Al^0-CNTs-Fe_3O_4.

Table 2
Thermodynamic parameters of SMZ adsorbed on Al^0-CNTs-Fe_3O_4

T (K)	$\Delta G°$ (kJ/mol)	$\Delta S°$ (kJ/(mol·K))	$\Delta H°$ (kJ/mol)
298	–12.494	0.01868	–8.902
308	–12.609		
318	–12.868		

Obviously, the SMZ adsorption onto Al^0-CNTs-Fe_3O_4 fitted well with the pseudo-second-order model due to the high correlation coefficients. Moreover, the calculated adsorption capacity (q_e) by the pseudo-second-order model was much closer to the experimental data (q_{exp}), which implied that the chemical adsorption was the rate-controlled step in the adsorption process [48].

3.3. Degradation of SMZ

3.3.1. Effects of solid to water ratio on the degradation of SMZ

The SMZ degradation efficiency of the Al^0-CNTs-Fe_3O_4/O_2 system was seriously affected by the solid to water ratio. As shown in Fig. 7, the SMZ degradation efficiency increased with the increase in the solid to water ratio. The highest degradation efficiency (100%) reached at a solid to water ratio of 3.0 g/L, which might be owing to the high solid to water ratio provided more available active sites for the activation of O_2. Moreover, high solid to water ratio

Table 1
Parameters of the four adsorption isotherm models

T (K)	Langmuir isotherm model			Freundich isotherm model			Temkin model			Dubinin–Radushkevich model		
	b (L/mg)	Q_{max} (mg/g)	R^2	n	K_F	R^2	K_t (L/mg)	B_1	R^2	Q_{max} (mg/g)	E (kJ/mol)	R^2
298	0.690	17.497	0.9982	5.180	8.047	0.9249	0.072	19.826	0.9764	19.372	17.832	0.9621
308	0.572	17.324	0.9978	2.645	4.089	0.9544	0.009	29.673	0.9122	13.621	16.523	0.9412
318	0.350	14.918	0.9952	1.731	6.297	0.8948	0.025	32.725	0.9333	13.028	17.100	0.9884

Table 3
Parameters of four kinetic models

C_0 (mg/L)	Pseudo-first-order kinetic model				Pseudo-second-order kinetic model			Intraparticle diffusion model		Elovich model	
	$q_{\exp}$ (mg/g)	k_1	q_e (mg/g)	R^2	k_2 (g/(mg min))	q_e (mg/g)	R^2	k_d (mg/(g min$^{1/2}$))	R^2	α_E (mg/g min)	R^2
5	5.819	0.368	5.467	0.9538	0.063	6.052	0.9952	5.585	0.9210	0.203	0.9362
10	8.405	0.875	7.509	0.6860	0.174	7.770	0.9858	4.923	0.9091	0.172	0.8831
25	12.931	1.295	12.443	0.8882	0.192	12.730	0.9943	6.382	0.9381	0.113	0.8933

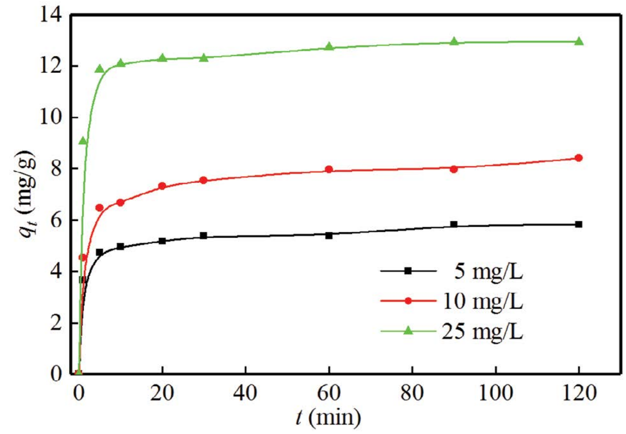

Fig. 6. Effects of contact time on Al^0-CNTs-Fe_3O_4 adsorption capacity (Al^0-CNTs-Fe_3O_4 dosage = 0.8 g/L, temperature = 298 K, and initial pH = 3).

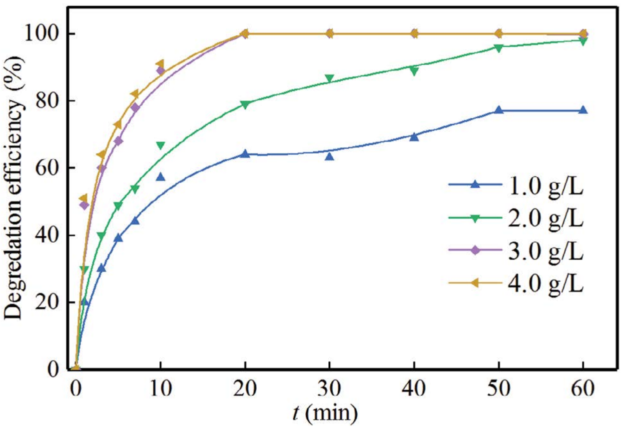

Fig. 7. Effects of solid to water ratio on SMZ degradation (SMZ concentration of adsorption = 2.5 mg/L, adsorbent dosage of adsorption = 0.8 g/L, initial adsorption pH = 3; degradation pH = 1.5, T = 298 K, initial degradation solution pH = 1.5).

could save the usage of acid for adjusting pH. However, the increase in the degradation efficiency of SMZ was limited when the solid to water ratio higher than 3 g/L, which might be due to that the less water in the system, the less O_2 could be transferred to the aqueous solution. Thus, the ratio of 3 g/L was selected for the subsequent experiments.

3.3.2. Degradation of SMZ by different processes

Batch control experiments were conducted to determine main oxidation species for the SMZ degradation by the Al^0-CNTs-Fe_3O_4/O_2 system at the initial SMZ concentration of 2.5 mg/L. In order to ensure the mass of CNTs in Al^0-CNTs and Al^0-CNTs-Fe_3O_4 were identical, the dosage of Al^0-CNTs in the Al^0-CNTs/O_2 system and the dosage of Al^0-CNTs-Fe_3O_4 in the Al^0-CNTs-Fe_3O_4/O_2 system were 2.55 and 3 g/L, respectively. The cumulative concentrations of H_2O_2 for Al^0-CNTs/O_2, Al^0-CNTs-Fe_3O_4/O_2, and Al^0-CNTs-Fe_3O_4/O_2/TBA systems at the O_2 flow rate of 200 mL/min are shown in Fig. 8a. The degradation efficiency of SMZ in the Al^0-CNTs/O_2 and the Al^0-CNTs-Fe_3O_4/O_2 systems are shown in Fig. 8b. O_2 was the precursor of the *in-situ* generation of H_2O_2 via reacting with Al^0-CNTs in the Al^0-CNTs-Fe_3O_4/O_2 system. A high concentration of H_2O_2 (131 mg/L) was observed in the Al^0-CNTs/O_2 system, but only 4.82% of SMZ was degraded in the system. This indicated that H_2O_2 and Al^0-CNTs/O_2 system had a limited oxidation capacity for SMZ. On the other hand, almost no H_2O_2 was detected in the Al^0-CNTs-Fe_3O_4/O_2 system that had the highest SMZ degradation efficiency, which implied that the Fe_3O_4 in Al^0-CNTs-Fe_3O_4 could decompose the H_2O_2 produced by the reaction of Al^0-CNTs in Al^0-CNTs-Fe_3O_4 with O_2 into species with strong oxidation capacity. Moreover, as a quencher of the $^{\bullet}$OH radical, TBA was added to the Al^0-CNTs-Fe_3O_4/O_2 system and leaded to almost no degradation removal of SMZ. This suggested that the $^{\bullet}$OH radicals played a key role in the SMZ degradation.

3.4. Comparison of two degradation removal processes of SMZ

The degradation efficiency of SMZ by the one-step and two-step processes are shown in Fig. 9. It was obvious that the degradation rate of the two-step process was faster than that of the one-step process. The degradation efficiency of SMZ by the two-step process reached 99.58% in 10 min, whereas the degradation efficiency only reached 68.53% by the one-step process. After 10 min, the equilibrium was achieved in the two-step process while the equilibrium was gradually achieved in the one-step process after 40 min. The advantages of the two-step process on the SMZ degradation might be owing to that the high concentration of SMZ on the surface of Al^0-CNTs-Fe_3O_4 in the two-step process enhanced the reaction driving force between SMZ and

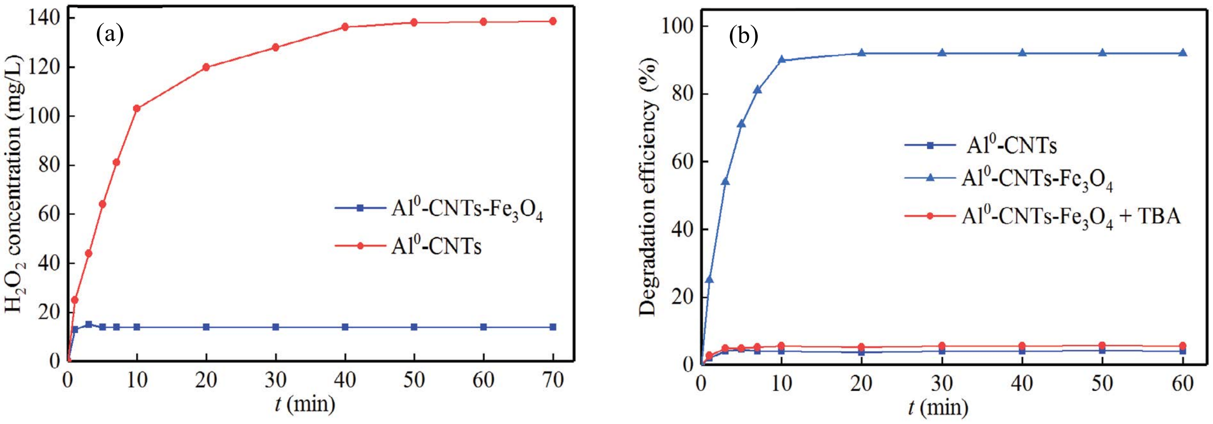

Fig. 8. (a) Cumulative H_2O_2 concentrations in two different systems; (b) degradation of SMZ in three systems (Al^0-CNTs-Fe_3O_4 = 3 g/L or Al^0-CNTs = 2.55 g/L, initial solution pH = 1.5, SMZ initial concentration = 2.5 mg/L, O_2 flow rate = 200 mL/min, and T = 298 K).

the •OH radical generated by the Al^0-CNTs-Fe_3O_4/O_2 system. Moreover, the degradation of SMZ by the Al^0-CNTs-Fe_3O_4/O_2 system needs the initial pH to be adjusted to 1.5, which requires large amount of acid if using the one-step process. However, the consumption of acid was reduced in the two-step process to achieve the similar degradation efficiency to that in the one-step process, due to the high solid to water ratio in the degradation of SMZ by the two-step process. Therefore, the two-step process has a better potential for removing low concentration SMZ in wastewater.

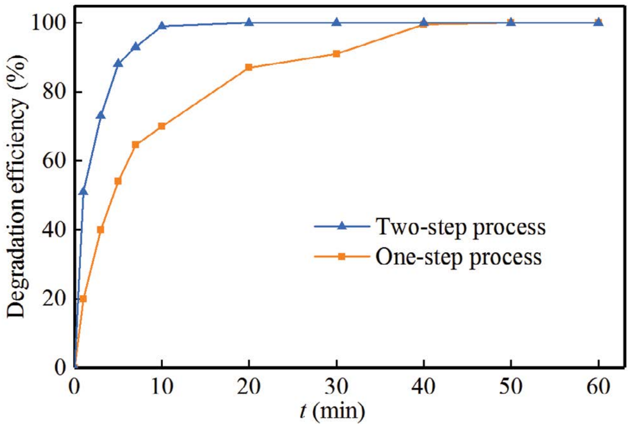

Fig. 9. Oxidation removal of SMZ by different processes (the one-step process: initial SMZ concentration = 2.5 mg/L, adsorbent dosage = 0.8 g/L, T = 298 K, initial pH = 1.5; the two-step process: initial SMZ concentration of adsorption = 2.5 mg/L, adsorbent dosage of adsorption = 0.8 g/L, initial adsorption pH = 3; solid to water ratio of degradation = 3 g/L, initial degradation pH = 1.5, and T = 298 K).

3.5. Proposed mechanism

3.5.1. Adsorption of SMZ on Al^0-CNTs-Fe_3O_4

Isotherm experiment results showed that the adsorption of SMZ onto Al^0-CNTs-Fe_3O_4 was dominated by a monolayer adsorption and the active sites were uniformly distributed on the surface of Al^0-CNTs-Fe_3O_4. The SEM spectrum and the BET analysis indicated that Al^0-CNTs-Fe_3O_4 had a large specific surface area and a porous structure, which resulted in an increase of the van der Waals force between Al^0-CNTs-Fe_3O_4 and SMZ. The FTIR spectrum confirmed that there were EDA interactions between the –NH and –NH_2 groups of SMZ and the CNTs of Al^0-CNTs-Fe_3O_4, and there might be n–π or π–π EDA interactions between the unshared pair of electrons of N or O (e.g., –NH_2, –O–) in SMZ and the CNTs as well [43]. Additionally, the effect of initial pH on the removal of SMZ had proved that electrostatic attraction was also responsible for the SMZ adsorption. As mentioned above, Al^0-CNTs-Fe_3O_4 showed broad affinity toward SMZ in solution, which resulted from the van der Waals force, chemical bonds, and electrostatic attraction between SMZ and the surface of Al^0-CNTs-Fe_3O_4.

3.5.2. Degradation of SMZ by Al^0-CNTs-Fe_3O_4

XRD and SEM analyses indicated that Al^0 and Fe_3O_4 existed on the surface of CNTs, Tan et al. [20] confirmed that the direct contact between Al^0 and CNTs would result in the formation of corrosion cells with Al^0 as the anode and CNTs as the cathode when Al^0-CNTs composite was added into the aqueous solution containing O_2. The mechanism of the oxidation process could be listed as follows (Eqs. (15)–(17)):

$$(\text{Anode}) \quad \text{Al-6e}^- \rightarrow 2\text{Al}^{3+} \tag{15}$$

$$(\text{Cathode}) \quad 3\text{O}_2 + 6\text{H}^+ + 6\text{e}^- \rightarrow 3\text{H}_2\text{O}_2 \tag{16}$$

$$2\text{Al} + 3\text{O}_2 + 6\text{H}^+ \rightarrow 2\text{Al}^{3+} + 3\text{H}_2\text{O}_2 \tag{17}$$

Based on the above electrode reactions, H_2O_2 would be generated *in-situ* in the solution. The H_2O_2 that produced in the Al^0-CNTs/O_2 system would be decomposed to •OH radical with strong oxidability by Fe_3O_4 (Eq. (18)) that has been reported in many literatures as an excellent Fenton-like catalyst [49–51]:

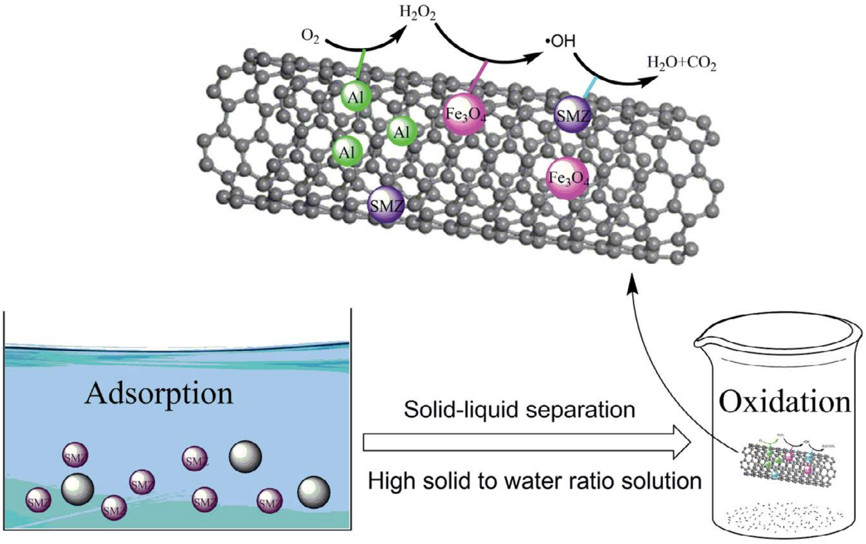

Fig. 10. Al^0-CNTs-Fe_3O_4 for the removal of SMZ by the two-step process.

$$Fe_3O_4 + H_2O_2 \rightarrow {}^{\bullet}OH \quad (18)$$

$^{\bullet}$OH radicals have been used extensively to degrade the refractory organic contaminants due to their 2.80 V high standard potential [52]. Therefore, it is reasonable to expect that the generated $^{\bullet}$OH radicals were involved in the degradation of SMZ.

3.5.3. Mechanism of the two-step removal of SMZ

The mechanism of the two-step removal of SMZ by Al^0-CNTs-Fe_3O_4 is shown in Fig. 10. In the two-step process, SMZ was firstly adsorbed on Al^0-CNTs-Fe_3O_4 through van der Waals force, electrostatic attraction and the formation of chemical bonds, etc., at initial pH of 3. Then the SMZ-saturated Al^0-CNTs-Fe_3O_4 was separated by a magnet and added into H_2SO_4 solution with initial pH of 1.5 and O_2 aeration for SMZ degradation. In the second step, O_2 was activated and converted to H_2O_2/$^{\bullet}$OH, and SMZ adsorbed on the surface of Al^0-CNTs-Fe_3O_4 was degraded by $^{\bullet}$OH radicals with strong oxidability.

4. Conclusions

The as-prepared Al^0-CNTs-Fe_3O_4 had a porous structure, large specific surface area, and abundant functional groups, which could adsorb SMZ through van der Waals forces, electrostatic attraction, and the formation of chemical bond. Moreover, O_2 could be activated by Al^0-CNTs-Fe_3O_4 to *in-situ* generated H_2O_2/$^{\bullet}$OH in solution for the degradation of SMZ. Thus, SMZ could be firstly adsorbed on Al^0-CNTs-Fe_3O_4 at the optimum condition and then be oxidized by Al^0-CNTs-Fe_3O_4/O_2 system with high solid to water ratio. This two-step process had higher degradation efficiency than one-step process, which was because SMZ adsorbed on Al^0-CNTs-Fe_3O_4 provided mass transfer dynamic for subsequent degradation; and with the two-step process, it is able to conduct the adsorption and degradation of SMZ at their respective optimal conditions. Overall, this two-step process has a good potential in the removal of refractory organic contaminants at trace or low concentrations.

Acknowledgments

The research was financially supported by the National Natural Science Foundation of China (No. 51878427).

References

[1] R. Hirsch, T. Ternes, K. Haberer, K.L. Kratz, Occurrence of antibiotics in the aquatic environment, Sci. Total Environ., 225 (1999) 109–118.

[2] L. Wu, Y. Song, M. Hu, X. Xu, H. Zhang, A. Yu, Q. Ma, Z. Wang, Determination of sulfonamides in butter samples by ionic liquid magnetic bar liquid-phase microextraction high-performance liquid chromatography, Anal. Bioanal. Chem., 407 (2015) 569–580.

[3] A.V. Herrera-Herrera, J. Hernández-Borges, M.M. Afonso, J.A. Palenzuela, M.Á. Rodríguez-Delgado, Comparison between magnetic and non magnetic multi-walled carbon nanotubes-dispersive solid-phase extraction combined with ultra-high performance liquid chromatography for the determination of sulfonamide antibiotics in water samples, Talanta, 116 (2013) 695–703.

[4] J. Wang, M. Gao, F. Ding, T. Shen, Organo-vermiculites modified by heating and gemini pyridinium surfactants: preparation, characterization and sulfamethoxazole adsorption, Colloids Surf., A, 546 (2018) 143–152.

[5] K. Chen, L. Liu, W. Chen, Adsorption of sulfamethoxazole and sulfapyridine antibiotics in high organic content soils, Environ. Pollut., 231 (2017) 1163–1171.

[6] L. Gao, Y. Shi, W. Li, H. Niu, J. Liu, Y. Cai, Occurrence of antibiotics in eight sewage treatment plants in Beijing, China, Chemosphere, 86 (2012) 665–671.

[7] J. Du, H. Zhao, S. Liu, H. Xie, Y. Wang, J. Chen, Antibiotics in the coastal water of the South Yellow Sea in China: occurrence, distribution and ecological risks, Sci. Total Environ., 595 (2017) 521–527.

[8] T. Wang, S. Ai, Y. Zhou, Z. Luo, C. Dai, Y. Yang, J. Zhang, H. Huang, S. Luo, L. Luo, Adsorption of agricultural wastewater contaminated with antibiotics, pesticides and toxic metals by functionalized magnetic nanoparticles, J. Environ. Chem. Eng., 6 (2018) 6468–6478.

[9] L.P. Bao, C.O. Chong, S.M.S. Mohamed, S. Pau-Loke, C. Jo-Shu, C.L. Tau, S.L. Su, C.J. Joon, Conventional and emerging technologies for removal of antibiotics from wastewater, J. Hazard. Mater., 400 (2020) 122961, doi: 10.1016/j.jhazmat.2020.122961.

[10] L. Clarizia, D. Russo, I. Di Somma, R. Marotta, R. Andreozzi, Homogeneous photo-Fenton processes at near neutral pH: A review, Appl. Catal., B, 209 (2017) 358–371.

[11] N. López, S. Plaza, A. Afkhami, P. Marco, J. Giménez, S. Esplugas, Treatment of diphenhydramine with different AOPs including photo-Fenton at circumneutral pH, Chem. Eng. J., 318 (2017) 112–120.

[12] R. Zhang, Y. Yang, C. Huang, L. Zhao, P. Sun, Kinetics and modeling of sulfonamide antibiotic degradation in wastewater and human urine by UV/H_2O_2 and UV/PDS, Water Res., 103 (2016) 283–292.

[13] P. Gong, H. Yuan, P. Zhai, Y. Xue, H. Li, W. Dong, G. Mailhot, Investigation on the degradation of benzophenone-3 by UV/H_2O_2 in aqueous solution, Chem. Eng. J., 277 (2015) 97–103.

[14] J. Tang, J. Wang, Fenton-like degradation of sulfamethoxazole using Fe-based magnetic nanoparticles embedded into mesoporous carbon hybrid as an efficient catalyst, Chem. Eng. J., 351 (2018) 1085–1094.

[15] Z. Xiu, Y. Cao, Z. Xing, T. Zhao, Z. Li, W. Zhou, Wide spectral response photothermal catalysis-fenton coupling systems with 3D hierarchical Fe_3O_4/Ag/Bi_2MoO_6 ternary hetero-superstructural magnetic microspheres for efficient high-toxic organic pollutants removal, J. Colloid Interface Sci., 533 (2019) 24–33.

[16] G.B. Ortiz De La Plata, O.M. Alfano, A.E. Cassano, Decomposition of 2-chlorophenol employing goethite as Fenton catalyst II: reaction kinetics of the heterogeneous Fenton and photo-Fenton mechanisms, Appl. Catal., B, 95 (2010) 14–25.

[17] J.M. Campos-Martin, G. Blanco-Brieva, J.L.G. Fierro, Hydrogen peroxide synthesis: an outlook beyond the anthraquinone process, Angew. Chem., Int. Ed., 45 (2006) 6962–6984.

[18] D. Kim, K.K. Sakimoto, D. Hong, P. Yang, Artificial photosynthesis for sustainable fuel and chemical production, Angew. Chem., Int. Ed., 54 (2015) 3259–3266.

[19] X. Gong, Z. Yang, L. Peng, A. Zhou, Y. Liu, Y. Liu, *In-situ* synthesis of hydrogen peroxide in a novel Zn-CNTs-O_2 system, J. Power Sources, 378 (2018) 190–197.

[20] N. Tan, Z. Yang, X. Gong, Z. Wang, T. Fu, Y. Liu, *In situ* generation of H_2O_2 using MWCNT-Al/O_2 system and possible application for glyphosate degradation, Sci. Total Environ., 650 (2019) 2567–2576.

[21] Z. Qiang, J. Chang, C. Huang, Electrochemical generation of hydrogen peroxide from dissolved oxygen in acidic solutions, Water Res., 36 (2002) 85–94.

[22] S. Siahrostami, A. Verdaguer-Casadevall, M. Karamad, D. Deiana, P. Malacrida, B. Wickman, M. Escudero-Escribano, E.A. Paoli, R. Frydendal, T.W. Hansen, I. Chorkendorff, I.E.L. Stephens, J. Rossmeisl, Enabling direct H_2O_2 production through rational electrocatalyst design, Nat. Mater., 12 (2013) 1137–1143.

[23] S. Yuan, Y. Fan, Y. Zhang, M. Tong, P. Liao, Pd-Catalytic *in situ* generation of H_2O_2 from H_2 and O_2 produced by water electrolysis for the efficient electro-Fenton degradation of Rhodamine B, Environ. Sci. Technol., 45 (2011) 8514–8520.

[24] B. Hayati, A. Maleki, F. Najafi, F. Gharibi, G. McKay, V.K. Gupta, S. Harikaranahalli Puttaiah, N. Marzban, Heavy metal adsorption using PAMAM/CNT nanocomposite from aqueous solution in batch and continuous fixed bed systems, Chem. Eng. J., 346 (2018) 258–270.

[25] G. Asgari, A. Seidmohammadi, J. Faradmal, A. Esrafili, M. Noori Sepehr, M. Jafarinia, Optimization of synthesis a new composite of nano-MgO, CNT and graphite as a catalyst in heterogeneous catalytic ozonation for the treatment of pesticide-laden wastewater, J. Water Process Eng., 33 (2020) 101082, doi: 10.1016/j.jwpe.2019.101082.

[26] Q. Zhou, X. Lin, B. Li, X. Luo, Fluoride adsorption from aqueous solution by aluminum alginate particles prepared via electrostatic spinning device, Chem. Eng. J., 256 (2014) 306–315.

[27] N. Nasseh, B. Barikbin, L. Taghavi, M.A. Nasseri, Adsorption of metronidazole antibiotic using a new magnetic nanocomposite from simulated wastewater (isotherm, kinetic and thermodynamic studies), Composites, Part B, 159 (2019) 146–156.

[28] D. Mohan, V.K. Gupta, S.K. Srivastava, S. Chander, Kinetics of mercury adsorption from wastewater using activated carbon derived from fertilizer waste, Colloids Surf., A, 177 (2001) 169–181.

[29] E.C. Lima, A. Hosseini-Bandegharaei, J.C. Moreno-Piraján, I. Anastopoulos, A critical review of the estimation of the thermodynamic parameters on adsorption equilibria. Wrong use of equilibrium constant in the Van't Hoof equation for calculation of thermodynamic parameters of adsorption, J. Mol. Liq., 273 (2019) 425–434.

[30] Y.Y. Sun, Q.Y. Yue, B.Y. Gao, Q.L, L.H. Huang, F.J. Yao, X. Xu, Preparation of activated carbon derived from cotton linter fibers by fused NaOH activation and its application for oxytetracycline (OTC) adsorption, J. Colloid Interface Sci., 368 (2012) 521–527.

[31] Y. Lin, D. Li, J. Hu, G. Xiao, X. Fu, Highly efficient photocatalytic degradation of organic pollutants by PANI-modified TiO_2 composite, J. Phys. Chem. C, 116 (2012) 5764–5772.

[32] Y. Liu, Q. Fan, S.X. Wang, Y. Liu, A.L. Zhou, L. Fan, Adsorptive removal of fluoride from aqueous solutions using Al-humic acid-La aerogel composites, Chem. Eng. J., 306 (2016) 174–185.

[33] A.A.M. Daifullah, B.S. Girgis, Impact of surface characteristics of activated carbon on adsorption of BTEX, Colloids Surf., A, 214 (2003) 181–193.

[34] H.K. Moghaddam, M. Pakizeh, Experimental study on mercury ions removal from aqueous solution by MnO_2/CNTs nanocomposite adsorbent, Ind. Eng. Chem., 21 (2015) 221–229.

[35] M.F.R. Pereira, S.F. Soares, J.J.M. Órfão, J.L. Figueiredo, Adsorption of dyes on activated carbons: influence of surface chemical groups, Carbon, 41 (2003) 811–821.

[36] Y.B. Liu, N. Tan, B.Q. Wang, Y. Liu, Stepwise adsorption–oxidation removal of oxytetracycline by Zn^0-CNTs-Fe_3O_4 from aqueous solution, Chem. Eng. J., 375 (2019) 121963, doi: 10.1016/j.cej.2019.121963.

[37] C. Lu, F. Su, Adsorption of natural organic matter by carbon nanotubes, Sep. Purif. Technol., 58 (2007) 113–121.

[38] S.G. Wang, X.W. Liu, W.X. Gong, N. Wei, B.Y. Gao, Q.Y. Yue, Adsorption of fulvic acids from aqueous solutions by carbon nanotubes, J. Chem. Technol. Biotechnol., 82 (2010) 698–704.

[39] H. Hoon, K. Jae-Hong, Natural organic matter (NOM) adsorption to multi-walled carbon nanotubes: effect of NOM characteristics and water quality parameters, Environ. Sci. Technol., 42 (2008) 4416–4421.

[40] Q. Liao, J. Sun, L. Gao, The adsorption of resorcinol from water using multi-walled carbon nanotubes, Colloids Surf., A, 312 (2008) 160–165.

[41] H. Milh, B. Schoenaers, A. Stesmans, D. Cabooter, R. Dewil, Degradation of sulfamethoxazole by heat-activated persulfate oxidation: elucidation of the degradation mechanism and influence of process parameters, Chem. Eng. J., 379 (2020) 122234, doi: 10.1016/j.cej.2019.122234.

[42] T. Golzari Aqda, S. Behkami, M. Raoofi, H. Bagheri, Graphene oxide-starch-based micro-solid phase extraction of antibiotic residues from milk samples, J. Chromatogr. A, 1591 (2019) 7–14.

[43] H. Zhao, X. Liu, Z. Cao, Y. Zhan, X. Shi, Y. Yang, J. Zhou, J. Xu, Adsorption behavior and mechanism of chloramphenicols, sulfonamides, and non-antibiotic pharmaceuticals on multi-walled carbon nanotubes, J. Hazard. Mater., 310 (2016) 235–245.

[44] H. Chen, B. Gao, H. Li, Removal of sulfamethoxazole and ciprofloxacin from aqueous solutions by graphene oxide, J. Hazard. Mater., 282 (2015) 201–207.

[45] I. Langmuir, The adsorption of gases on plane surfaces of glass, mica and platinum, J. Am. Chem. Soc., 40 (1918) 1361–1403.

[46] L.I. Ya-Jing, X.F. Sun, Y.E. Qing, B.C. Liu, W.U. Yao-Guo, Preparation and properties of a novel hemicellulose-based magnetic hydrogel, Acta Phys. Chim. Sin., 30 (2014) 111–120.

[47] G. McKay, M.J. Bino, A.R. Altamemi, The adsorption of various pollutants from aqueous solutions on to activated carbon, Water Res., 19 (1985) 491–495.

[48] L. Wang, L. Yang, Y. Li, Y. Zhang, X. Ma, Z. Ye, Study on adsorption mechanism of Pb(II) and Cu(II) in aqueous solution using PS-EDTA resin, Chem. Eng. J., 163 (2010) 364–372.

[49] H.L. So, K.Y. Lin, W. Chu, Triclosan removal by heterogeneous Fenton-like process: studying the kinetics and surface chemistry of Fe_3O_4 as catalyst, J. Environ. Chem. Eng., 7 (2019) 103432, doi: 10.1016/j.jece.2019.103432.

[50] A. Tolba, M. Gar Alalm, M. Elsamadony, A. Mostafa, H. Afify, D.D. Dionysiou, Modeling and optimization of heterogeneous Fenton-like and photo-Fenton processes using reusable Fe_3O_4-MWCNTs, Process Saf. Environ. Prot., 128 (2019) 273–283.

[51] Y. Liu, Q. Fan, J.L. Wang, Zn-Fe-CNTs catalytic *in situ* generation of H_2O_2 for Fenton-like degradation of sulfamethoxazole, J. Hazard. Mater., 342 (2017) 166–176.

[52] V.L. Pham, D.G. Kim, S.O. Ko, Oxidative degradation of the antibiotic oxytetracycline by Cu@Fe_3O_4 core-shell nanoparticles, Sci. Total Environ., 631–632 (2018) 608–618.